Theoretical study of the Compton effect with correlated three-photon emission: From the differential cross section to high-energy triple-photon entanglement

Erik Lötstedt[1,*] and Ulrich D. Jentschura[2,3]

[1] *Laser Technology Laboratory, RIKEN Advanced Science Institute, 2-1 Hirosawa, Wako, Saitama 351-0198, Japan*
[2] *Department of Physics, Missouri University of Science and Technology, Rolla, Missouri 65409-0640, USA*
[3] *MTA–DE Particle Physics Research Group, P.O.Box 51, H–4001 Debrecen, Hungary*

The three-photon Compton effect is studied. An incoming photon undergoes triple scattering off a free electron, which leads to the emission of three entangled photons. We investigate the properties of both the total cross section, assuming a low-energy cutoff for the detected photons, and the differential cross section. Particular emphasis is laid on evaluating polarization-resolved cross sections. The entanglement of the final three-photon state is analyzed.

PACS numbers: 34.50.-s, 12.20.Ds, 03.65.Ud

arXiv:1405.1669v1 [quant-ph] 7 May 2014

I. INTRODUCTION

A photon colliding with a free electron is one of the most basic processes of quantum electrodynamics (QED). At low photon energies ω_0 (in the rest frame of the electron), the only possible process is the scattering of the incoming photon off the electron. The electron-positron pair production threshold is at $\omega_0 = 4m$, which is larger than $2m$ due to the necessity of providing for the minimum electron recoil momentum. (Here, m is the mass of the electron. Throughout this article, we work in natural units such that $\hbar = c = \epsilon_0 = 1$, and $\alpha = e^2/4\pi$, where $\alpha \approx 1/137.036$ is the fine-structure constant and e the charge of the electron.) Moreover, for $\omega_0 \ll m$, the scattering is elastic and referred to as Thomson scattering. In this limit, the Klein-Nishina cross section [1] calculated from quantum electrodynamics (QED) agrees with the prediction from classical electrodynamics. When ω_0 becomes comparable to m or above, the scattering process is termed Compton scattering, or just the Compton effect [2]. It has to be described in fully relativistic QED [3, 4].

Compton scattering has been widely studied, and has a large number of applications. By analyzing the broadening of the Compton peak (the Compton profile) of the scattered photons, information on the electron momentum distribution in atoms [5, 6], molecules [7] and condensed matter [8–10] can be obtained. Compton scattering from bound electrons can in general be described by the Klein-Nishina cross section if the energy gained by the electron is much larger than the binding energy, which implies that the electron can be regarded as free during the collision. It is also possible to produce high-energy gamma photons through Compton backscattering of laser photons off of energetic electrons from an accelerator. The (non-exhaustive list of) review articles [11–14] discuss applications of the Compton effect. There also exists a nonlinear generalization of the Compton effect: in a laser field, several photons are absorbed by an electron to produce one final photon. The electron-laser interaction has to be taken into account beyond perturbation theory. This nonlinear process has received a lot of interest recently, both theoretically [15–17] and experimentally [18, 19].

Much less studied are the processes where a photon collides with an electron and splits into two or more final-state photons. Such a reaction is of higher order in α and has a smaller cross section. One should not confuse this kind of scattering process with multiple single Compton scattering events, which can occur when a photon scatters consecutively at different electrons inside a material [20]. This paper exclusively deals with the process involving one electron and one photon in the initial state, and a final state consisting of one electron and one, two or three photons.

At moderate energies $\omega_0 \sim m$, the cross sections of the higher-order processes are suppressed with one factor of α for each additional emitted photon. A complete QED calculation of the double Compton effect, where two photons are emitted, was first presented in [21], and has since been verified experimentally by several groups [22–28]. The total double Compton cross section, for some particular photon energy infrared cutoff, has been studied theoretically by numerical integration [29]. The theory of the nonlinear (multi-photon) double Compton effect (in the background of a strong laser field) has been given only recently [30–33].

The next-order Compton process is the triple, or three-photon Compton effect, where one photon is split into three after the collision with a free electron. A rather sophisticated pertinent experiment has been described in Ref. [34]; otherwise the experimental literature on triple scattering appears to be scarce. In Ref. [34], the differential cross section (averaged over the detector solid angles) was estimated for one specific arrangement of the detection geometry of the emitted photons. The three detectors were arranged in a symmetric configuration and each detector covered a narrow solid angle $\Omega \ll 4\pi$. On the theoretical side, the literature also is very scarce. In Ref. [35], the total cross section for the n-tuple Compton effect was studied for extremely high photon energies

* lotstedt@chem.s.u-tokyo.ac.jp

$\omega_0 \gg m$ (in the rest frame of the electron). At moderate energies $\omega_0 \sim m$, which could more realistically be achieved in the laboratory, we have recently presented calculations of the total and differential cross section for a number of examples of experimentally realizable parameter sets [36]. It is the purpose of the present paper to extend the parameter range covered in Ref. [36] and to give the details of the method of calculation which could be useful if the method is to be adapted to a particular experimental geometry in the future.

Compton scattering with multiple photons in the final state is interesting for an additional reason: The final photons are quantum mechanically entangled. The experimental production of multi-photon entangled states is currently at the focus of intense research efforts [37–46]. One can say that the three-photon Compton process is the most basic QED process that is able to produce a three-photon entangled final state. A somewhat related process is electron-positron annihilation into three photons. This process has been studied both in high-energy physics with colliding e^+ and e^- beams [47–52] and in the low-energy domain in the context of the decay of orthopositronium as a test of CP violation [53–58]. Higher-order QED corrections to the decay rate have been calculated [59–63]. The discrepancy between the experimental results of the Tokyo group [64, 65] and the Michigan group [66–68] was finally resolved in Ref. [69].

We proceed as follows. In Sec. II, we describe the QED theory necessary to obtain expressions for the differential cross sections for the two-photon and three-photon Compton effect. A numerical evaluation of the total cross section is presented in Sec. III B, and examples of the differential cross section are presented in Secs. III C and III D. The interesting subject of polarization entanglement among the three final state photons is discussed in Sec. IV, and we conclude in Sec. V.

II. THEORY

A. Bispinors and photon states

In the following, we write the scalar product of two four-vectors a and b as $a \cdot b \equiv a^\mu b_\mu = a^0 b^0 - \vec{a} \cdot \vec{b}$, which also defines the metric convention. The contraction of a four-vector a with the Dirac gamma matrices γ^μ is denoted as $\hat{a} = \gamma^\mu a_\mu = a^0 \gamma^0 - \vec{a} \cdot \vec{\gamma}$.

The incoming and outgoing four-vectors of the electron are labeled as

$$p_{i,f} = (E_{i,f}, \vec{p}_{i,f}) \,, \tag{1}$$

respectively. The electron bispinors are used in the representation [4]

$$u_r(p) = \sqrt{\frac{E+m}{2m}} \begin{pmatrix} \delta_{r1} \\ \delta_{r2} \\ \dfrac{1}{E+m} \vec{\sigma} \cdot \vec{p} \begin{pmatrix} \delta_{r1} \\ \delta_{r2} \end{pmatrix} \end{pmatrix}, \tag{2}$$

where δ_{ij} is the Kronecker delta, $r = 1$ or 2 labels the spin of the electron, and the vector $\vec{\sigma}$ is composed of the (Pauli) 2×2 spin matrices,

$$\vec{\sigma} = \left(\begin{bmatrix} 0 & 1 \\ 1 & 0 \end{bmatrix}, \begin{bmatrix} 0 & -\mathrm{i} \\ \mathrm{i} & 0 \end{bmatrix}, \begin{bmatrix} 1 & 0 \\ 0 & -1 \end{bmatrix} \right). \tag{3}$$

With this convention, the spinors are normalized according to $u_r^\dagger(p) \gamma^0 u_r(p) = \bar{u}_r u_r = 1$. Here, $\bar{u}_r = u_r^\dagger \gamma^0$ is the Dirac adjoint. The gamma matrices are used in the Dirac representation,

$$\gamma^0 = \begin{pmatrix} \mathbb{1} & 0 \\ 0 & -\mathbb{1} \end{pmatrix}, \qquad \gamma^i = \begin{pmatrix} 0 & \sigma^i \\ -\sigma^i & 0 \end{pmatrix}, \tag{4}$$

for $i = 1, 2, 3$, where $\mathbb{1}$ denotes the 2×2 unit matrix, and the σ^i are the components of the vector of Pauli matrices. The propagation wave vectors (four-vectors) of the photons are denoted as

$$k_j = (\omega_j, \vec{k_j}) = \omega_j (1, \sin\theta_j \cos\phi_j, \sin\theta_j \sin\phi_j, \cos\theta_j), \tag{5}$$

where ϕ_j measures the azimuth and θ_j measures the polar angle ($j = 0, 1, 2, 3$). We take $j = 0$ to denote the (incoming) absorbed photon, and $j = 1, 2, 3$ to denote the emitted photons. We furthermore define

$$n_j = \frac{k_j}{|\vec{k_j}|} = (1, \sin\theta_j \cos\phi_j, \sin\theta_j \sin\phi_j, \cos\theta_j), \tag{6}$$

so that the four-vector k_j is given as $k_j = \omega_j n_j$. In all examples presented in Sec. III, the angles and energies of the final particles are measured in the lab frame, in a coordinate system with the polar axis defined by the incoming photon, i.e., $k_0 = \omega_0(1, 0, 0, 1)$. A head-on collision such that $p_i = (E_i, 0, 0, -\sqrt{E_i^2 - m^2})$ is always assumed.

We now give the basis for the two polarization four-vectors ϵ_j^1 and ϵ_j^2 of the photons ($j = 1, 2, 3$, each outgoing photon has two polarizations available). These four-vectors satisfy $\epsilon_j^1 \cdot k_j = \epsilon_j^2 \cdot k_j = 0$ (for each j individually, no sum over j) and are needed to analyze the polarization-resolved cross sections. We take them as

$$\begin{aligned} \epsilon_j^1 &= (0, \vec{\epsilon}_j^{\,1}) = (0,\, \cos\theta_j \cos\phi_j,\, \cos\theta_j \sin\phi_j,\, -\sin\theta_j) \,, \\ \epsilon_j^2 &= (0, \vec{\epsilon}_j^{\,2}) = (0,\, -\sin\phi_j,\, \cos\phi_j,\, 0) \,. \end{aligned} \tag{7}$$

The superscript denotes either one of the two available polarizations.

B. Matrix element and differential cross section

The expression for the cross section of the three-photon Compton effect follows in a straightforward way from the usual Feynman rules of QED [3, 4]. The expression for the invariant matrix element M_{TC} reads (TC stands for triple Compton)

$$M_{\mathrm{TC}} = \frac{1}{4} \frac{e^4 N_{\mathrm{TC}}}{(2\pi)^5} \frac{1}{m^2 \sqrt{E_i E_f \omega_0 \omega_1 \omega_2 \omega_3}} \,, \tag{8}$$

with

$$N_{\rm TC} = m^3 \sum_\zeta u^\dagger_{r_f}(p_f)\gamma^0 \hat\epsilon_{\zeta(3)} \frac{\hat q_3(\zeta)+m}{q_3^2(\zeta)-m^2} \hat\epsilon_{\zeta(2)} \frac{\hat q_2(\zeta)+}{q_2^2(\zeta)-}$$
$$\times\, \hat\epsilon_{\zeta(1)} \frac{\hat q_1(\zeta)+m}{q_1^2(\zeta)-m^2} \hat\epsilon_{\zeta(0)} u_{r_i}(p_i).$$

In Eq. (9), the sum runs over all the 4! = 24 availa permutations ζ of $(0,1,2,3)$ and describes the boso symmetrization of the final state. One might th that, because of the presence of three indistinguisha particles in the final state, an additional combina rial factor should have to be taken into account. deed, a factor 1/3! must be inserted if we seek to cal late the total cross section for the triple scattering p cess (see Sec. III B below), roughly speaking, because "wide-angle detectors" needed for the theoretical cal lation of the total cross section (with overlapping acc tor solid angles) would otherwise detect the same pho more than once. There is no need to add such a facto the differential cross section. We here include this c sideration because it might be important for experime in the future.

Let us also give an example for the permutations entering Eq. (9): E.g., if $\zeta = (2,3,1,0)$, then $\zeta(0) = 2$, $\zeta(1) = 3$, $\zeta(2) = 1$, $\zeta(3) = 0$, and so on. The momenta q_n entering the propagators are calculated according to the equation

$$q_n(\zeta) = p_i + \sum_{j=0}^{n-1} (-1)^{1-\delta_{0\zeta(j)}} k_{\zeta(j)}\,, \tag{10}$$

which describes the momentum flow through the diagram (δ_{ij} is the Kronecker delta). The zeroth photon with propagation four-vector k_0 adds to the momentum flow, while the three emissions with k_j $(j = 1,2,3)$ need to be subtracted. Each one of the terms in Eq. (9) corresponds to one Feynman diagram, three of which are exemplified in Fig. 1.

According to the Feynman rules of QED, the differential cross section follows from the matrix element (8) as

$$\frac{{\rm d}\sigma}{{\rm d}\omega_1 {\rm d}\omega_2 {\rm d}\omega_3 {\rm d}^3 p_f {\rm d}\Omega_1 {\rm d}\Omega_2 {\rm d}\Omega_3} = \tag{11}$$
$$(2\pi)^2 \frac{E_i\,\omega_0}{p_i\cdot k_0} |M_{\rm TC}|^2\, \omega_1^2\, \omega_2^2\, \omega_3^2\, \delta^{(4)}(p_i + k_0 - \sum_{j=1}^3 k_j - p_f),$$

where ${\rm d}\Omega_j = {\rm d}\phi_j {\rm d}\theta_j \sin\theta_j$ is the infinitesimal solid angle of photon j. In (11), both the integrations over ${\rm d}^3 p_f$ and ${\rm d}\omega_3$ can be taken with the aid of the delta function, to

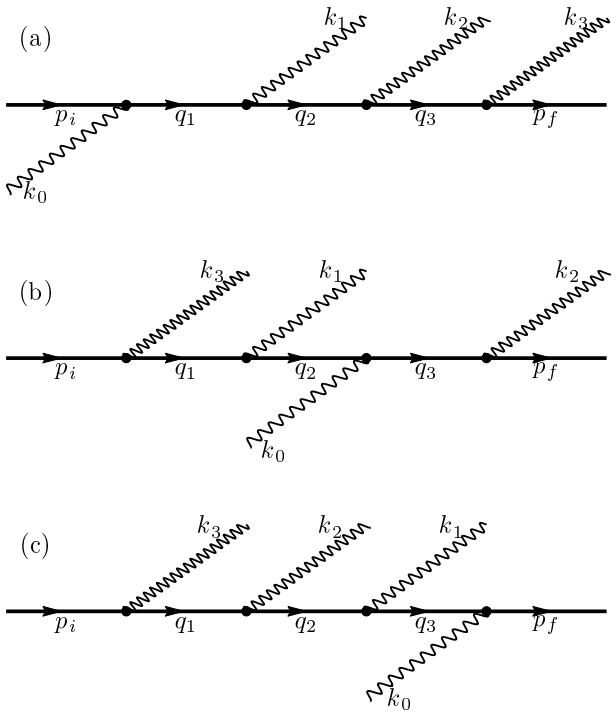

FIG. 1. Three Feynman diagrams out of the total of 4! = 24 which contribute to the three-photon Compton effect. Diagram (a) corresponds to the permutation $\zeta = (0,1,2,3)$, diagram (b) to the permutation $\zeta = (3,1,0,2)$, and diagram (c) to the permutation $\zeta = (3,2,1,0)$.

yield

$$\vec p_f = \vec p_i + \vec k_0 - \sum_{j=1}^3 \vec k_j\,, \tag{12a}$$

$$E_f = E_i + \omega_0 - \sum_{j=1}^3 \omega_j\,, \tag{12b}$$

$$\omega_3 = \frac{p_i\cdot(k_1+k_2-k_0) + k_0\cdot(k_1+k_2) - k_1\cdot k_2}{n_3\cdot(k_1+k_2-k_0-p_i)}. \tag{12c}$$

For fixed values of the angles θ_j, ϕ_j, the condition $\omega_3 > 0$ defines the area of the $\omega_1\omega_2$ plane in which the differential cross section is nonvanishing; otherwise it is zero due to kinematic constraints. The integration over ${\rm d}\omega_3$ introduces an additional factor

$$\frac{{\rm d}(E_f+\omega_3)}{{\rm d}\omega_3} = 1 + \frac{\vec n_3\cdot(\vec k_1+\vec k_2-\vec k_0-\vec p_i)+\omega_3}{E_f}. \tag{13}$$

The final expression for the differential cross section of the three-photon Compton effect, differential in the 6 angles and 2 energies of the emitted photons, still dependent on the one incoming and three outgoing photon polariza-

tions, and the electron spins, reads (in natural units)

$$\frac{\mathrm{d}\sigma_{\mathrm{TC}}}{\mathrm{d}\omega_1\,\mathrm{d}\omega_2\,\mathrm{d}\Omega_1\,\mathrm{d}\Omega_2\,\mathrm{d}\Omega_3} = \frac{\alpha^4}{(2\pi)^4}\frac{1}{m^4}\frac{\omega_1\omega_2\omega_3}{E_f\,(p_i\cdot k_0)} \times\left|\left(\frac{\mathrm{d}(E_f+\omega_3)}{\mathrm{d}\omega_3}\right)^{-1}\right| |N_{\mathrm{TC}}|^2\,\Theta(\omega_3)\,\Theta(E_f-m). \tag{14}$$

In Eq. (14), ω_3 should be replaced according to Eq. (12c), and p_f is to be replaced according to $p_f = p_i + k_0 - \sum_{j=1}^{3} k_j$. The step functions $\Theta(\cdot)$ at the end of Eq. (14) are needed since there are values for the angles that result in $\omega_3 > 0$ from Eq. (12c), but $E_f < m$.

The cross section (14) diverges whenever either ω_1, ω_2 or ω_3 goes to zero. This is the well-known infrared catastrophe of QED. In the current case, the divergences would cancel against fourth-order (in α) radiative corrections to the single and double Compton effect. The radiated energy, which is proportional to $\int \mathrm{d}\omega_1 \int \mathrm{d}\omega_2 \int \mathrm{d}\omega_3\, \omega_1\omega_2\omega_3 \mathrm{d}\sigma_{\mathrm{TC}}/(\mathrm{d}\Omega_1\mathrm{d}\Omega_2\mathrm{d}\Omega_3\mathrm{d}\omega_1\mathrm{d}\omega_2\mathrm{d}\omega_3)$ is still finite when integrated in the infrared. While certainly an interesting subject of study [70–73], such corrections will not be considered in the present paper. In general, radiative corrections to the cross section are expected to be of order α, or at the few-percent level, since we consider photon energies (in the rest frame of the electron) of at most $\omega_0 = 100$ MeV in this paper (see Sec. III B on the total cross section). At high energy $\omega_0 \gg m$, infrared radiative corrections can be shown to be the dominant ones [72]. The bremsstrahlung corrections in the exit channel, which are cancelled by the radiative corrections in the infrared, are in our case of the order $c_{\mathrm{IR}} = (\alpha/\pi)\ln(2\omega_0/m)\ln(2\omega_0 m/\Delta^2)$, where Δ is the energy resolution of the detector. The precise value therefore depends on the experimental setup [72]. Assuming that $\omega_0/\Delta = 100$, then $c_{\mathrm{IR}} \approx 0.06$ for $\omega_0 = 100$ MeV. In all our examples for the differential cross section in Secs. III C and III D, however, the energy scale is much smaller. In the electron rest frame, we have $\omega_0/m \approx 0.4$ in Sec. III C and $\omega_0/m \approx 1$ in Sec. III D. In this case we expect $c_{\mathrm{IR}} = (\alpha/\pi)\ln(2m^2/\Delta^2) \approx 0.02$. So, the radiative corrections are expected not to exceed the level of a few percent.

Let us dwell on this point a little longer, assuming the latter situation, where $c_{\mathrm{IR}} \sim (\alpha/\pi)\ln(m/\Delta)$ up to multiplicative factors. The theorem of Yennie, Frautschi and Suura [72] as well as the considerations of Sudakov [71] imply that, if the calculation were carried through to infinite loop order, the infrared divergences exponentiate according to

$$\sum_{n=0}^{\infty}\frac{(-1)^n}{n!}\left[\frac{\alpha}{\pi}\ln\left(\frac{m}{\Delta}\right)\right]^n = \exp\left[-\frac{\alpha}{\pi}\ln\left(\frac{m}{\Delta}\right)\right], \tag{15}$$

but, if the calculation is carried out only to a finite loop order, then the next higher-order terms (in α) will yield radiative and bremsstrahlung corrections on the percent level.

In an experiment, the detectors are always set up such as to detect photons above a certain infrared threshold energy. For example, the experiment in Ref. [34] detected photons with an energy greater than 13 keV. Theoretically, we do the same thing, i.e., when integrating over the energy, we only include photon energies larger than a fixed energy threshold which we label ε. Let us put $\omega_3 = \varepsilon$ in Eq. (12c). We can then calculate the maximum energy $\omega_1^{\max}$ of ω_1 as a function of all the other variables using $k_1 = \omega_1 n_1$ and solving for ω_1. Let us investigate fixed emission angles and photon energies ω_ℓ, where $\ell = 2$ if $j = 1$, and $\ell = 1$ if $j = 2$ (formally, $\ell = 3 - j$). Then, one obtains for the maximimum energy $\omega_j^{\max}$ of the jth photon the expression

$$\omega_j^{\max} = \frac{\varepsilon n_3\cdot(k_\ell - p_i - k_0) + p_i\cdot k_0 - k_\ell\cdot(p_i + k_0)}{n_j\cdot(p_i + k_0 - k_\ell - \varepsilon n_3)}. \tag{16}$$

The differential cross section integrated over the final photon energies will depend on the infrared cutoff ε. Furthermore, since the specification of an energy threshold depends on the observer frame, total cross sections are no longer Lorentz invariant, but the applicable threshold is fixed by the properties of the detectors used.

C. Comparison to the double Compton effect

In order to compare the cross section for the three-photon Compton effect with that of the double Compton effect, we now take a step back, and first give the expressions for the double (two-photon) Compton differential cross section. Although there exists an analytic expression for the polarization- and spin-summed cross section [21], there is no analytic expression available for the polarization-resolved cross section. The matrix element for the double Compton (DC) effect reads

$$M_{\mathrm{DC}} = e^3\frac{1}{(2\pi)^{\frac{7}{2}}}\frac{1}{m\sqrt{8E_iE_f\omega_0\omega_1\omega_2}}N_{\mathrm{DC}}, \tag{17}$$

with

$$N_{\mathrm{DC}} = m^2\sum_{\chi} u_{r_f}(p_f)\gamma^0\hat{\epsilon}_{\chi(2)}\frac{\hat{q}_2(\chi)+m}{q_2^2(\chi)-m^2} \times\hat{\epsilon}_{\chi(1)}\frac{\hat{q}_1(\chi)+m}{q_1^2(\chi)-m^2}\hat{\epsilon}_{\chi(0)}u_{r_i}(p_i), \tag{18}$$

where the sum runs over all the $3! = 6$ permutations χ of $(0,1,2)$. The momenta q_n entering the propagators are defined similarly to the three-photon Compton case as

$$q_n(\chi) = p_i + \sum_{j=0}^{n-1}(-1)^{1-\delta_{0\chi(j)}}k_{\chi(j)}, \tag{19}$$

i.e. the zeroth photon momentum flows in, the others flow out. The cross section, differential in ω_1, Ω_1 and

Ω_2, follows in analogy with Eq. (14) above as

$$\frac{\mathrm{d}\sigma_{\mathrm{DC}}}{\mathrm{d}\omega_1 \mathrm{d}\Omega_1 \mathrm{d}\Omega_2} = \frac{\alpha^3}{(2\pi)^2} \frac{1}{m^2} \frac{\omega_1 \omega_2}{E_f\,(p_i \cdot k_0)} \left| \left(\frac{\mathrm{d}(E_f + \omega_2)}{\mathrm{d}\omega_2} \right)^{-1} \right| \times |N_{\mathrm{DC}}|^2 \Theta(\omega_2) \Theta(E_f - m). \tag{20}$$

In (20), the final momentum of the electron is $p_f = p_i + k_0 - k_1 - k_2$, and

$$\omega_2 = \frac{p_i \cdot (k_1 - k_0) + k_0 \cdot k_1}{n_2 \cdot (k_1 - p_i - k_0)}. \tag{21}$$

The Dirac-δ function generates a Jacobian factor of $\mathrm{d}(E_f+\omega_2)/\mathrm{d}\omega_2 = 1+[\omega_2+\vec{n}_2\cdot(\vec{k}_1-\vec{p}_i-\vec{k}_0)]/E_f$. The double Compton cross section is used for comparison to the triple Compton effect in the following. The infrared cutoff ε is used in complete analogy to the triple-Compton process.

III. NUMERICAL EXAMPLES

A. Orientation

We now return to the three-photon Compton effect, while using the discussion of the double (two-photon) Compton scattering process from Sec. II C as a guide toward the comparison with lower-order processes. We thus numerically evaluate a number of examples of both the differential and the total cross section for experimentally realizable values of the parameters. The evaluation of the cross section is performed entirely numerically, assuming the representations given in Eqs. (2) and (4) for the gamma matrices and the electron spinors. Given the input parameters ω_0, E_i, ϵ_0, and ϵ_j, θ_j, ϕ_j, $j = 1, 2, 3$ (electron spin is always summed over), the evaluation of the matrix element is done by *explicit* matrix multiplication using the standard Dirac representation of the Clifford algebra given in Eq. (4). This method is far preferable, because an analytic evaluation of the cross section by tracing out the Dirac-γ matrices would result in an extremely long analytic expression which would not simplify (because we are investigating the differential cross section) and thus not be useful. The necessity to avoid an "explosion" in the number of terms in the intermediate expressions is particularly important, because we are interested in polarization-resolved cross sections, in which case there are no simplifications at all in the analytic trace. On the occasion, we also recall arguments given by us previously in Ref. [74] which demonstrate that, for typical multiple scattering processes, it is computationally faster to evaluate the matrix element by direct numerical matrix multiplication than to evaluate the analytic expressions that would otherwise result from the Dirac-γ matrix trace.

One test of correctness of the numerical implementation of the cross section is that of gauge invariance. The cross section (14) is invariant under the gauge transformation

$$\epsilon_j \to \epsilon_j + A\, k_j, \tag{22}$$

for each $j = 1, 2, 3$ separately. Here, A is an arbitrary constant.

In the numerical integration of the differential cross section, the integration over ω_1 and ω_2 is done by a standard Romberg routine. By contrast, the integration over the emission angles of the photons is performed by Monte Carlo integration [75]. Monte Carlo integration is a well-established method for QED processes with a many-dimensional final state phase space [76, 77], pioneered by Mork [78, 79].

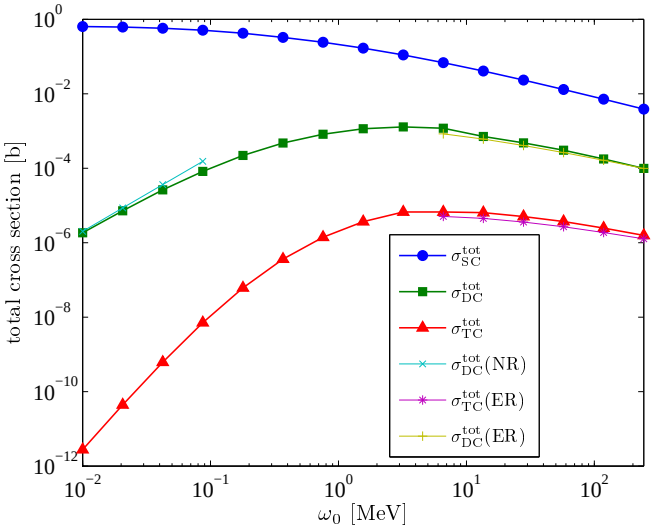

FIG. 2. (Color online) The total cross section σ^{tot} is plotted as a function of the initial photon energy ω_0, for the single (SC), double (DC), and triple (TC) Compton effect. The unit of barn is given as $1\,\mathrm{b} = 10^{-24}\,\mathrm{cm}^2 \approx 389.4^{-1}\,\mathrm{MeV}^{-2}$. The non-relativistic (NR) DC approximation is from Ref. [80], and the extreme relativistic (ER) approximations are taken from Ref. [35]. It is assumed that $E_i = m$ and that the photon energy threshold is $\varepsilon = \omega_0/50$. Note the doubly logarithmic scale.

B. Total cross section for n-fold scattering

In order to get an impression of the order of magnitude of the total number of three-photon events produced in an experiment, we first calculate the total cross section

$$\sigma^{\mathrm{tot}}_{\mathrm{TC}} = \frac{1}{3!4} \sum_{\text{spin, pol.}} \int \mathrm{d}\Omega_1 \mathrm{d}\Omega_2 \mathrm{d}\Omega_3 \times \int\limits_{\omega_{1,2,3} > \varepsilon} \mathrm{d}\omega_1 \mathrm{d}\omega_2 \frac{\mathrm{d}\sigma_{\mathrm{TC}}}{\mathrm{d}\omega_1 \mathrm{d}\omega_2 \mathrm{d}\Omega_1 \mathrm{d}\Omega_2 \mathrm{d}\Omega_3}, \tag{23}$$

averaged over initial polarization and spin, and summed over final state polarization and spin. Here, in contrast

to the differential cross section, the factor of $1/3! = 1/6$ is inserted to compensate for the double-counting of equivalent angular configurations. The electron is assumed to be initially at rest, $E_i = m$, and we assume the threshold $\varepsilon = \omega_0/50$. We aim to compare to the total double Compton cross section,

$$\sigma_{\rm DC}^{\rm tot} = \frac{1}{2!4} \sum_{\rm spin,\,pol.} \int {\rm d}\Omega_1 {\rm d}\Omega_2 \int\limits_{\omega_{1,2}>\varepsilon} {\rm d}\omega_1 \frac{{\rm d}\sigma_{\rm DC}}{{\rm d}\omega_1 {\rm d}\Omega_1 {\rm d}\Omega_2}, \tag{24}$$

and the total cross section $\sigma_{\rm SC}^{\rm tot}$ of the usual, single Compton (SC) effect, which is known analytically as [3]

$$\sigma_{\rm SC}^{\rm tot} = 2\pi \frac{\alpha^2}{m^2} \left\{ \frac{1+\omega}{\omega^3} \left[\frac{2\omega(1+\omega)}{1+2\omega} - \ln(1+2\omega) \right] + \frac{\ln(1+2\omega)}{2\omega} - \frac{1+3\omega}{(1+2\omega)^2} \right\}, \tag{25}$$

with $\omega = \omega_0/m$. As is well known, this cross section approaches a constant in the limit $\omega \to 0$, which reads as

$$\sigma_{\rm SC}^{\rm tot} = \frac{8\pi\alpha^2}{3m^2} \left[1 - 2\,\omega + \mathcal{O}\left(\omega^2\right) \right]. \tag{26}$$

The constant limit for $\omega_0 \to 0$ can be discerned in Fig. 2, where we show the total cross sections for the single (SC), double (DC), and triple (TC) Compton effect. For the DC case, we have included a comparison with the nonrelativistic result from Ref. [80],

$$\sigma_{\rm DC}^{\rm tot}({\rm NR}) = C_{\rm DC}^{\rm NR} \frac{\alpha^3}{m^2} \left(\frac{\omega_0}{m} \right)^2. \tag{27}$$

With our convention of $\varepsilon = \omega_0/50$ for the photon energy threshold, the constant $C_{\rm DC}^{\rm NR} \approx 9.1$. For TC, a numerical fit of the calculated points for $\omega_0 < 0.1\,{\rm MeV}$ gives $\sigma_{\rm TC}^{\rm tot} \propto \omega_0^n$ with $n \approx 3.6$. For low energies $\omega_0 \ll m$, $\sigma_{\rm TC}^{\rm tot}$ should be proportional to ω_0^4/m^6, like

$$\sigma_{\rm TC}^{\rm tot}({\rm NR}) = C_{\rm TC}^{\rm NR} \frac{\alpha^4}{m^2} \left(\frac{\omega_0}{m} \right)^4. \tag{28}$$

By matching expression (28) with $\sigma_{\rm TC}^{\rm tot}$ calculated at $\omega_0 = 10^{-2}$ MeV (the leftmost point in Fig. 2), we obtain $C_{\rm TC}^{\rm NR} \approx 4.5$ for the constant prefactor.

In the extreme relativistic (ER) limit, the total cross sections for the two-photon and three-photon Compton effect have been calculated in [35] in the approximation $\omega_0 \gg m$, $\omega_1 \gg m$, $\omega_j \ll m$ for $j > 1$, and $\omega_0 \gg \omega_1$. The result is [35]

$$\sigma^{\rm tot}({\rm ER}) = \frac{1}{n!} \left[\frac{\alpha}{\pi} \ln\left(\frac{2\omega_0}{m} \right) \ln\left(\frac{\varepsilon_{\rm up}}{\varepsilon_{\rm low}} \right) \right]^n \sigma_{\rm SC}^{\rm tot}, \tag{29}$$

where $n = 1$ for DC and $n = 2$ for TC, and $\varepsilon_{\rm low,up}$ are the lower and upper limits for the energy of the soft photons $\omega_{j>1}$. The result (29) is interesting, since it implies that at extremely high energies, the total cross sections of DC and TC can exceed that of SC. However, the energy scale at which this occurs is so high (the energy scale is of the order of the Landau pole in QED), so that this question is rather academic. Although the assumptions leading to the formula (29) do not hold in our case, since we assume that the photon energy threshold varies with the incoming photon energy as $\varepsilon = \omega_0/50$, and the soft-photon requirement $\omega_{j>1} \ll m$ becomes impossible to satisfy at high energies, we have still included the total cross section obtained from Eq. (29) in Fig. 2. In calculating $\sigma_{\rm DC,TC}^{\rm tot}({\rm ER})$, we assumed that $\varepsilon_{\rm up}/\varepsilon_{\rm low} = 5$. We can see from Fig. 2 that the expression (29) well approximates the calculated $\sigma_{\rm DC,TC}^{\rm tot}$ for $\omega_0 \gtrsim 10\,{\rm MeV}$. The decrease in the cross section with increasing ω_0 in the fully relativistic regime is due to the fact that

$$\sigma_{\rm SC}^{\rm tot} \approx \frac{\pi\alpha^2}{m} \frac{1}{\omega_0} \ln\left(\frac{2\omega_0}{m} \right) \tag{30}$$

for large $\omega_0 \gg m$. Numerically, our values for $\sigma_{\rm DC}^{\rm tot}$ disagree with those calculated in [29], but one has to be aware that in Ref. [29], a different convention for the photon energy threshold is employed.

From Fig. 2, we can infer a few interesting facts. Contrary to $\sigma_{\rm SC}^{\rm tot}$, which monotonically decreases with increasing ω_0, $\sigma_{\rm DC}^{\rm tot}$ and $\sigma_{\rm TC}^{\rm tot}$ peak at a certain value of $\omega_0 = \omega_0^{\rm max}$. The data in Fig. 2 roughly give the same value of $\omega_0^{\rm max} = 3.2\,{\rm MeV}$ for both DC and TC, with $\sigma_{\rm DC}^{\rm tot}(\omega_0^{\rm max}) = 1 \times 10^{-3}\,{\rm b}$ and $\sigma_{\rm TC}^{\rm tot}(\omega_0^{\rm max}) = 7 \times 10^{-6}\,{\rm b}$.

C. 180 keV photons on stationary electrons

Our first example for the differential cross section is taken at $\omega_0 = 180$ keV, $\varepsilon = \omega_0/50$, and $E_i = m$. This situation seems favorable for an experimental verification of the three-photon Compton effect which goes beyond that in Ref. [34], since photons of this energy are available at synchrotron radiation sources [81] with a high photon flux, and stationary targets allow for a high electron density. The total cross section is calculated to be $\sigma_{\rm TC}^{\rm tot} = 6 \times 10^{-8}\,{\rm b}$, which is rather low, but can be compensated for by the aforementioned high photon flux and large number of target electrons. If we assume a photon flux of $2 \times 10^{12}/{\rm s}$ (see Ref. [81]), and a 0.1 mm thick Al foil as the target, then we obtain about 900 photon triplets per second.

In Fig. 3, we show the differential cross section as a function of ω_1 and ω_2, for fixed emission angles of the photons and a particular set of final polarization vectors. For plotting purposes, we define the dimensionless quantity S as

$$S = \log_{10} \left(\frac{1}{2} \sum_{\rm spin} \frac{{\rm d}\sigma_{\rm TC}}{{\rm d}\Omega_1 {\rm d}\Omega_2 {\rm d}\Omega_3 {\rm d}\omega_1 {\rm d}\omega_2} \frac{{\rm MeV}^2\,{\rm sr}^3}{\rm b} \right), \tag{31}$$

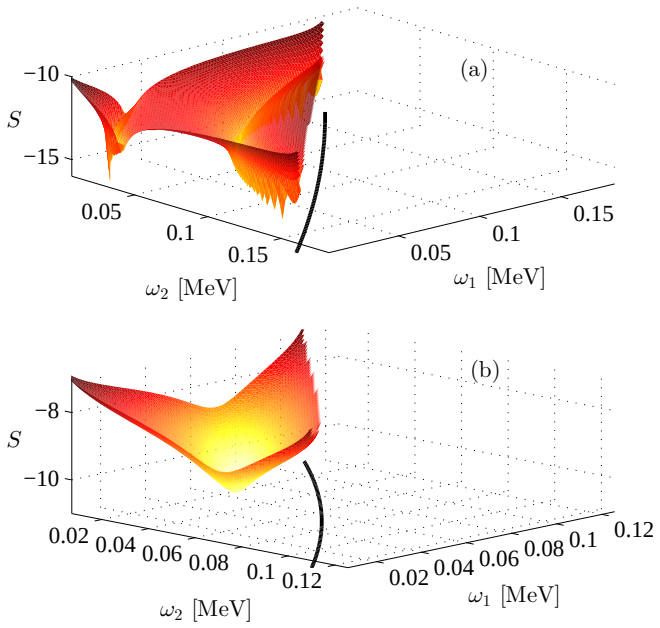

FIG. 3. (Color online) Differential cross section as a function of ω_1 and ω_2. We have $\omega_0 = 180$ keV, $E_i = m$, $\varepsilon = \omega_0/50$, and $\phi_j = 2j\pi/3$, $j = 1, 2, 3$. The value of the polar angle is $\theta_{1,2,3} = 1/2$ in panel (a) and $\theta_{1,2,3} = 2$ in panel (b), which corresponds to a triple scattering events in the forward and backward cones, respectively (relative to the incoming photon). The actual quantity plotted is S (the decadic logarithm of the differential cross section), as defined in Eq. (31). For the polarizations of the final photons, we have $(\vec{\epsilon}_1, \vec{\epsilon}_2, \vec{\epsilon}_3) = (\vec{\epsilon}_1^{\,1}, \vec{\epsilon}_2^{\,1}, \vec{\epsilon}_3^{\,1})$ in both panels, and the incoming photon is polarized in the x-direction. The thick, black line shows the curve along which the energy of photon three is at the assumed detector threshold, $\omega_3 = \varepsilon = 3.6$ keV. This curve can be calculated according to Eq. (16).

i.e., the decadic logarithm of the differential cross section averaged over the incoming, and summed over the outgoing electron spin, in units of $\mathrm{b\,MeV^{-2}\,sr^{-3}}$. For later use we also define the corresponding polarization-summed quantity

$$\overline{S} = \log_{10}\left(\frac{1}{2}\sum_{\text{spin, pol.}} \frac{\mathrm{d}\sigma_{\mathrm{TC}}}{\mathrm{d}\Omega_1\mathrm{d}\Omega_2\mathrm{d}\Omega_3\mathrm{d}\omega_1\mathrm{d}\omega_2}\frac{\mathrm{MeV^2\,sr^3}}{\mathrm{b}}\right), \tag{32}$$

where both electron spins and photon polarizations are summed over. In Fig. 3, the azimuthal angles of the three detectors are assumed to describe a "Mercedes-star" configuration with $\phi_j = 2j\pi/3$ for $j = 1, 2, 3$. The spin of the electron is summed over. For those values of ω_1 and ω_2 which would otherwise give rise to $\omega_3 < \varepsilon$ according to Eq. (12c), we have set the differential cross section to zero. The line at which $\omega_3 = \varepsilon$ (indicated with a thick, black line in Fig. 3) can be calculated with the help of Eq. (16). In the current case, we have $n_1 \cdot (p_i + k_0 - \varepsilon n_3) \gg n_1 \cdot k_2$, which implies that the denominator in Eq. (16) is almost constant, and consequently $\omega_1^{\max}(\omega_2)$ becomes an almost linear function of ω_2.

Measuring the 5-fold differential cross section of the three-photon Compton effect would require fixing three photon detectors at different positions in space and in addition applying a spectrometer. We can see that the patterns in the $\omega_1\omega_2$ plane and the overall magnitude of the differential cross section are different by several orders of magnitude depending on whether the final photons are emitted in a typical region within the forward cone [$\theta = 1/2$, Fig. 3(a)] or in the backward cone relative to the incoming photon [$\theta = 2$, Fig. 3(b)].

In Fig. 4, we present the differential cross section integrated over energy,

$$\frac{\mathrm{d}\sigma_{\mathrm{TC}}}{\mathrm{d}\Omega_1\mathrm{d}\Omega_2\mathrm{d}\Omega_3} = \frac{1}{2}\sum_{\text{spin}} \int\limits_{\omega_1,\omega_2,\omega_3>\varepsilon} \mathrm{d}\omega_1\mathrm{d}\omega_2 \times \frac{\mathrm{d}\sigma_{\mathrm{TC}}}{\mathrm{d}\Omega_1\mathrm{d}\Omega_2\mathrm{d}\Omega_3\mathrm{d}\omega_1\mathrm{d}\omega_2}, \tag{33}$$

and similarly for DC. The polarization-resolved differential cross section for SC is known analytically. For $E_i = m$, we have [3]

$$\frac{\mathrm{d}\sigma_{\mathrm{SC}}}{\mathrm{d}\Omega_1} = \frac{1}{4}\left(\frac{\alpha}{m}\right)^2\left(\frac{\omega_1}{\omega_0}\right)^2\left(\frac{\omega_1}{\omega_0} + \frac{\omega_0}{\omega_1} - 2 + 4(\vec{\epsilon}_1\cdot\vec{\epsilon}_0)\right), \tag{34}$$

where $\omega_1 = \omega_0/[1 + (\omega_0/m)(1 - \cos\theta_1)]$.

D. Laser photons on GeV electrons

In this example, we exploit the kinematics of a Compton backscattering setup, which would allow for the creation of entangled photon triplets in the GeV range. The incoming electron is no longer at rest. We take an ultrarelativistic electron beam with $E_i = 50$ GeV, and a visible laser photon beam with $\omega_0 = 2.5$ eV (corresponding to a laser wavelength of 496 nm). These parameters are close to those of the well-known experiment [82] performed at SLAC more than 15 years ago. Here, we have in mind laser pulses which are not intense enough to induce relativistic multi-photon processes, so that the scattering of a single laser photon gives the dominant contribution to the cross section. This limits the laser intensity to $I \lesssim 10^{17}$ W/cm^2. In terms of the classical nonlinear parameter $\xi = |e|F_{\mathrm{peak}}/(\omega_0 m)$, where F_{peak} is the peak electric field of the laser [83], we have $\xi \approx 0.1$ for $I = 10^{17}$ W/cm^2 at a $\omega_0 = 2.5$ eV laser light. We also note that despite the high value of E_i, the incoming photon energy ω_0' in the rest frame of the electron is $\omega_0' \approx 2\omega_0 E_i/m = 0.5$ MeV, which is below the $\mathrm{e^+\,e^-}$ pair production threshold of $4m \approx 2$ MeV, so that there is no background connected with the creation of $\mathrm{e^+\,e^-}$ pairs. Strong-field (multi-photon) pair production [76, 83, 84]

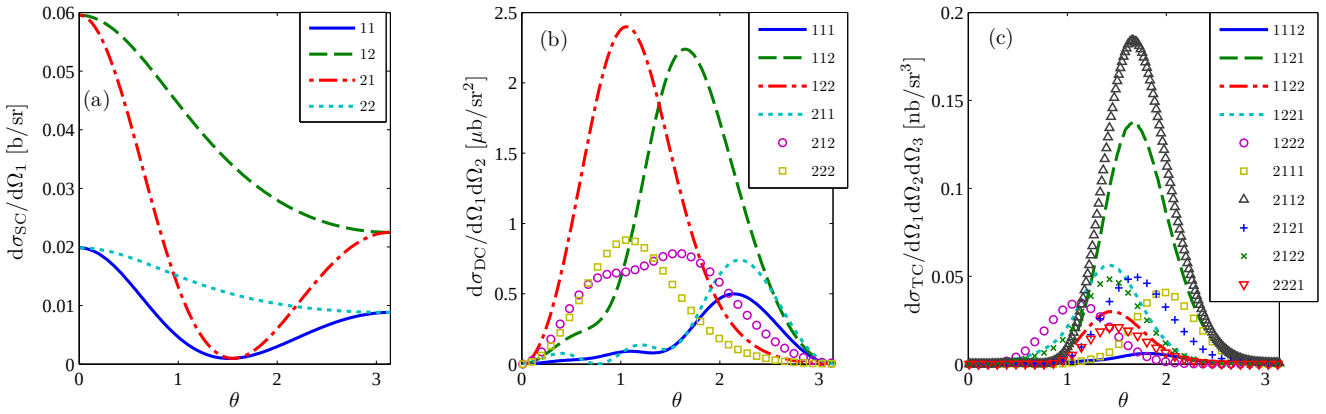

FIG. 4. (Color online) Comparison of the (a) single, (b) double, and (c) triple Compton differential cross sections at $\omega_0 = 180$ keV, $E_i = m$, integrated over photon energies larger than $\varepsilon = \omega_0/50$. It is assumed that $\theta_j = \theta$, $\phi_j = 2j\pi/3$, with $j = 1$ for SC, $j = 1, 2$ for DC, and $j = 1, 2, 3$ for TC. The indices ij, ijk, and $ijk\ell$ in the legends indicate the polarizations of the photons as $(\vec{\epsilon}_0, \vec{\epsilon}_1, \vec{\epsilon}_2, \vec{\epsilon}_3) = (\vec{\epsilon}_0^{\,i}, \vec{\epsilon}_1^{\,j}, \vec{\epsilon}_2^{\,k}, \vec{\epsilon}_3^{\,\ell})$ for TC, and correspondingly for DC and SC (with $i, j, k, \ell = 1, 2$). For symmetry reasons, in DC [panel (b)], 121 has the same curve as 112, and 221 has the same curve as 212. Similarly, in TC [panel (c)], 1111 has the same curve as 2111, $1212 = 1122$, $1211 = 1121$, $1222 = 2222$, $2211 = 2121$, and $2212 = 2122$.

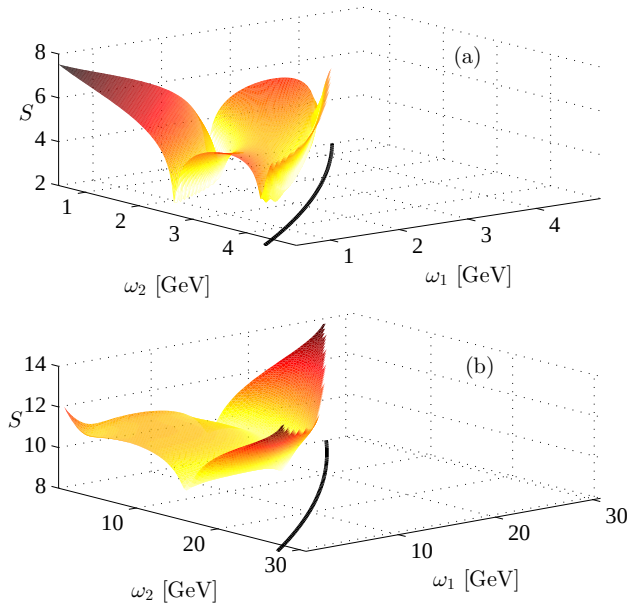

FIG. 5. (Color online) Differential cross section as a function of ω_1 and ω_2. We have $\omega_0 = 2.5$ eV, $E_i = 50$ GeV, $\varepsilon = E_i/100$, and $\phi_j = 2j\pi/3$ (again, a "Mercedes-star" configuration of the detectors), for $j = 1, 2, 3$. In panel (a), we have $\theta_{1,2,3} = \pi - 4\times10^{-5}$, and in (b), $\theta_{1,2,3} = \pi - 7\times10^{-6}$. For visualization purposes, the decadic logarithm S [defined in Eq. (31)] of the differential cross section is shown. The polarizations of the final photons are given as $(\vec{\epsilon}_1, \vec{\epsilon}_2, \vec{\epsilon}_3) = (\vec{\epsilon}_1^{\,2}, \vec{\epsilon}_2^{\,2}, \vec{\epsilon}_3^{\,1})$, while the incoming photon is polarized in the x-direction. The black, thick line corresponds to the curve along which the energy of photon three is at the assumed detector threshold, $\omega_3 = \varepsilon = 500$ MeV.

can also be neglected, since the strong-field QED parameter $\chi = \xi k_0 \cdot p_i/m^2 \approx 0.1$ is much smaller than unity.

In this situation, due to the high gamma factor $\gamma_i = E_i/m$ of the electron beam, the photons are emitted in a narrow cone $\theta_j \sim \pi - 1/\gamma_i$ around the axis of the incoming electron momentum $\vec{p}_i$. In addition, the emitted photons can acquire high energy, the maximum energy for emission in the backward direction being given by the relativistic limit of the Compton formula as $4\omega_0\gamma_i^2$.

The evaluation of the differential cross section becomes numerically problematic due to the extreme parameter values, if the calculation is performed in the laboratory frame. It is instead advantageous to perform the numerical calculation in the frame where the electron is initially at rest, and then Lorentz transform the computed quantities into the laboratory frame. Differential cross sections transform as

$$\frac{\mathrm{d}\sigma_{\mathrm{TC}}}{\mathrm{d}\Omega_1\mathrm{d}\Omega_2\mathrm{d}\Omega_3\mathrm{d}\omega_1\mathrm{d}\omega_2} = J^{-1}\,\frac{\mathrm{d}\sigma'_{\mathrm{TC}}}{\mathrm{d}\Omega'_1\mathrm{d}\Omega'_2\mathrm{d}\Omega'_3\mathrm{d}\omega'_1\mathrm{d}\omega'_2}, \quad (35)$$

with the relativistic Jacobian

$$J = \frac{(1-\beta_i^2)^2}{(1-\beta_i\cos\theta'_1)\,(1-\beta_i\cos\theta'_2)\,(1-\beta_i\cos\theta'_3)^2}, \quad (36)$$

where we have denoted rest-frame quantities with a prime, and $\beta_i = \sqrt{1-1/\gamma_i^2}$. For cross sections differential only in the angles we have instead the Jacobian

$$\tilde{J} = \frac{(1-\beta_i^2)^3}{(1-\beta_i\cos\theta'_1)^2\,(1-\beta_i\cos\theta'_2)^2\,(1-\beta_i\cos\theta'_3)^2}. \quad (37)$$

The photon energy threshold ε is still fixed in the laboratory frame. Therefore, when doing the integration over ω'_1 and ω'_2, we set the cross section to zero if the lab-frame value of the photon energy is below the threshold,

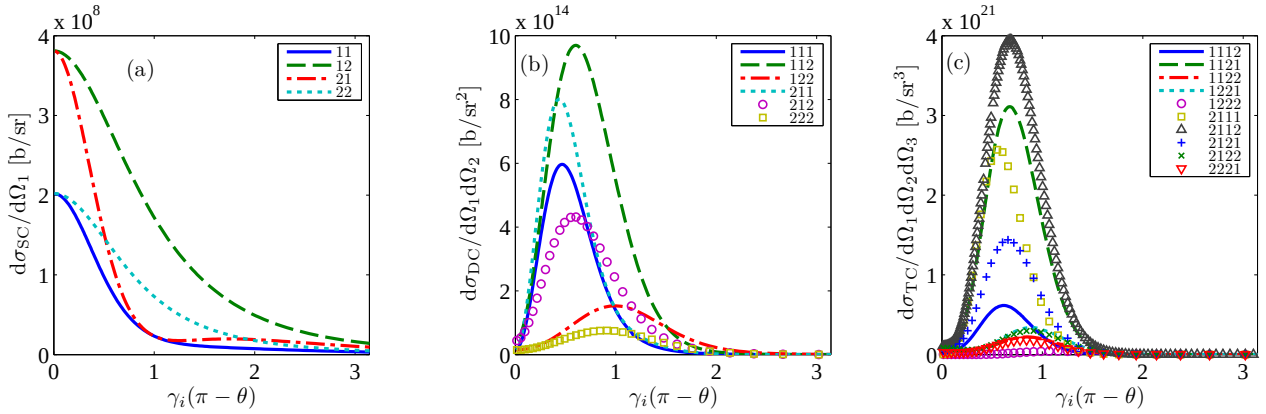

FIG. 6. (Color online) Comparison of the (a) single, (b) double, and (c) triple Compton differential cross sections at $\omega_0 = 2.5$ eV, $E_i = 50$ GeV (backscattering from an incoming electron) in the laboratory frame, integrated over photon energies larger than $\varepsilon = E_i/100$. It is assumed that $\theta_j = \theta$, $\phi_j = 2j\pi/3$, with $j = 1$ for the SC, $j = 1, 2$ for the DC, and $j = 1, 2, 3$ for the TC effect. The differential cross sections are plotted against $\gamma_i(\pi - \theta)$, where $\gamma_i = E_i/m \approx 9.8 \times 10^4$, and $\gamma_i(\pi - \theta) = 0$ implies that the photons are completely backscattered, i.e., emitted anti-parallel to the incoming photon. The indices ij, ijk, and $ijk\ell$ in the legends indicate the polarizations of the photons as $(\vec{\epsilon}_0, \vec{\epsilon}_1, \vec{\epsilon}_2, \vec{\epsilon}_3) = (\vec{\epsilon}_0^{\,i}, \vec{\epsilon}_1^{\,j}, \vec{\epsilon}_2^{\,k}, \vec{\epsilon}_3^{\,\ell})$ for TC, and correspondingly for DC and SC (with $i, j, k, \ell = 1, 2$). For symmetry reasons, in DC [panel (b)], 121 has the same curve as 112, and 221 has the same curve as 212. Similarly, in TC [panel (c)], 1111 has the same curve as 2111, $1212 = 1122$, $1211 = 1121$, $1222 = 2222$, $2211 = 2121$, and $2212 = 2122$. Note also that in (c), the 2221 curve almost overlaps the 1122 curve, and the 2122 curve almost overlaps the 1221 curve.

i.e., we impose the condition

$$\omega_j = \gamma_i(1 - \beta_i \cos\theta_j')\,\omega_j' > \varepsilon\,, \tag{38}$$

for $j = 1, 2, 3$.

Because the values for the total cross section shown in Fig. 2 only apply to an electron at rest, and with a different convention for the photon energy threshold, we have calculated anew the total cross section for the current example. We get

$$\sigma_{\rm TC}^{\rm tot} = 6 \times 10^{-7}\,{\rm b} \tag{39}$$

for $\omega_0 = 2.5$ eV, $E_i = 50$ GeV, and $\varepsilon = E_i/100 = 500$ MeV. The value (39) coincides with the value of $\sigma_{\rm TC}^{\rm tot}(\omega_0' = 0.5\,{\rm MeV}, E_i = m) = 6 \times 10^{-7}$ b, which can be obtained from interpolation of the points in Fig. 2. Assuming an electron bunch containing 10^9 electrons, a laser intensity of 10^{17} W/cm^2, a pulse length of 100 fs, and perfect transverse overlap of the laser pulse and the electron bunch, we obtain about 15 triple photon events per collision.

Examples of the fully differential cross section in the laboratory frame are shown in Fig. 5. The differential cross sections integrated over the final photon energies are displayed in Fig. 6. Due to the small value of the Jacobian (37) at large γ_i, the DC and TC differential cross sections become very large in the lab frame. However, numerically, the total, integrated cross section for the triple scattering is not large [see Eq. (39)].

IV. MULTIPARTITE ENTANGLEMENT

The three photons in the final state of the triple Compton effect are emitted coherently, during the same coherence interval, and they are therefore quantum mechanically correlated, or entangled. Currently, a lot of effort is being invested into the creation of controllable entangled quantum states of three or more particles in the laboratory [37, 38]. The conventional way of creating double or triple states of entangled photons is by nonlinear down-conversion in a crystal [39–42, 44–46], while it is only recently that direct production of a triple photon state was successful [43]. With the current study, we propose the three-photon Compton effect as an alternative source of entangled triplets of photons. No nonlinear medium is required. Whether or not the three-photon Compton effect is going to be effective as a source of entangled photons depends on the experimental setup and the optimization thereof. Here, we limit ourselves to pointing out that the emitted three photons are entangled, and to an investigation of the degree of entanglement.

In principle, the emitted photons are entangled in all of their physical degrees of freedom: energies, angles, and polarization. The case which has been mostly investigated in other areas so far is that of entangled qubits, i.e., of entangled states within a well-defined manifold of discrete states (such as spin or polarization states). Here, therefore, we study the polarization entanglement of the photons. The starting point is the density matrix

ρ, which has elements

$$\langle\lambda_1\lambda_2\lambda_3|\rho|\lambda_1'\lambda_2'\lambda_3'\rangle = \kappa\sum_{\text{spin}} M_{\text{TC}}(\lambda_1\lambda_2\lambda_3)M_{\text{TC}}^*(\lambda_1'\lambda_2'\lambda_3'). \tag{40}$$

The invariant matrix element for triple scattering M_{TC} is given in Eq. (8). The prefactor κ is fixed by the normalization condition $\text{Tr}\,\rho = 1$. We have written

$$M_{\text{TC}}(\lambda_1\lambda_2\lambda_3) = M_{\text{TC}}(\vec{\epsilon}_1 = \vec{\epsilon}_1^{\,\lambda_1}, \vec{\epsilon}_2 = \vec{\epsilon}_2^{\,\lambda_2}, \vec{\epsilon}_3 = \vec{\epsilon}_3^{\,\lambda_3}), \tag{41}$$

with $\lambda_j \in \{1, 2\}$. When the state vectors $|\lambda_1\lambda_2\lambda_3\rangle$ are expressed as column vectors with $2^3 = 8$ entries, the density matrix ρ becomes an 8×8 matrix.

Given a density matrix ρ, it is a highly non-trivial problem to determine whether ρ contains genuine multipartite entanglement or not [85–92]. A $2 \times 2 \times 2$ system like the current one is considered to be genuinely multipartite entangled if its density matrix ρ cannot be written in the form [89]

$$\begin{aligned}\rho = {} & p_1 \sum_j q_1^j |\Lambda_1^j\rangle\langle\Lambda_1^j| \otimes |\Gamma_{23}^j\rangle\langle\Gamma_{23}^j| + \\ & p_2 \sum_j q_2^j |\Lambda_2^j\rangle\langle\Lambda_2^j| \otimes |\Gamma_{13}^j\rangle\langle\Gamma_{13}^j| + \\ & p_3 \sum_j q_3^j |\Lambda_3^j\rangle\langle\Lambda_3^j| \otimes |\Gamma_{12}^j\rangle\langle\Gamma_{12}^j|,\end{aligned} \tag{42}$$

where p_j, q_ℓ^j are positive numbers satisfying $\sum_{j=1}^3 p_j = \sum_j q_\ell^j = 1$ for any $\ell = 1, 2, 3$. A state vector $|\Gamma_{k\ell}^j\rangle$ represents a general entangled state of photon k and ℓ, while a state $|\Lambda_n^j\rangle$ denotes a general one-photon state of photon n. Intuitively, a state ρ is considered to be tripartite entangled if it cannot be written as a sum of states that can be factorized into states with less entanglement. However, given a density matrix ρ, there is currently no efficient algorithm to decide whether or not ρ can be written in the form (42).

In Refs. [88, 89], an algorithm was proposed, which is able to detect "almost all" genuinely tripartite entangled states. It works as follows. Under the condition that the matrices $\mathcal{P}_s$, $\mathcal{Q}_s$, $\mathbb{1} - \mathcal{P}_s$ and $\mathbb{1} - \mathcal{Q}_s$ do not have any negative eigenvalues (which can be written in short form as $0 \le \mathcal{P}_s,\ \mathcal{Q}_s \le \mathbb{1}$), we search for the maximum value of

$$\tau(\rho) = -\,\text{Tr}(W\rho) \tag{43}$$

by varying $\mathcal{P}_s$ and $\mathcal{Q}_s$, where W is assumed to be a function of $\mathcal{P}_s$ and $\mathcal{Q}_s$. Because $\mathbb{1} - \mathcal{P}_s$ and $\mathbb{1} - \mathcal{Q}_s$ have no negative eigenvalues, in particular, one cannot take the entries of $\mathcal{P}_s$ to be arbitarily large and positive, since then $\mathbb{1} - \mathcal{P}_s$ would have negative eigenvalues. In concrete terms, the entanglement witness W in (43) is given as

$$W = \mathcal{P}_s + \mathcal{Q}_s^{T_s} \tag{44}$$

for all subsets $s \in \{1, 2, 3, 12, 13, 23\}$, and T_s denotes the partial transpose with respect to the subset s [93]. If we write

$$\varrho = \sum_{ijk\ell mn=1}^{2} \varrho_{ijk\ell mn} |i\rangle\langle j| \otimes |k\rangle\langle\ell| \otimes |m\rangle\langle n| \tag{45}$$

for a generic density matrix, then, for example, the partial transpose with respect to $s = 3$ is

$$\varrho^{T_3} = \sum_{ijk\ell mn=1}^{2} \varrho_{ijk\ell mn} |i\rangle\langle j| \otimes |k\rangle\langle\ell| \otimes |n\rangle\langle m|, \tag{46}$$

and similarly for other values of s. In general, an entanglement witness W is a Hermitian matrix such that the trace $\text{Tr}(W\rho)$ is negative for at least one entangled state ρ, and positive for all non-entangled states. The normalization of W is limited by the positive eigenvalue condition $0 \le \mathcal{P}_s,\ \mathcal{Q}_s \le \mathbb{1}$. If one is only interested in detecting whether ρ is entangled or not, and no quantitative measure of entanglement is needed, the condition $\mathcal{P}_s,\ \mathcal{Q}_s \le \mathbb{1}$ is replaced with the normalization condition $\text{Tr}\,W = 1$ [88, 89]. If the maximum of $-\,\text{Tr}(W\rho)$ with $W = \mathcal{P}_s + \mathcal{Q}_s^{T_s}$ for all s is positive, the state ρ is genuinely entangled. It was shown in [88, 89] that an entanglement witness on the form (44) can be used to detect a large class of genuinely entangled states which are not so-called PPT mixtures. However, there are some genuinely entangled states that are not detected by the algorithm. The form (44) moreover permits the optimization of (43) to be solved by the methods of convex optimization theory, for which there exist standard software packages [94]. We refer to [88, 89] for further details about the algorithm.

The value of $\tau(\rho)$ is a measure of the tripartite entanglement present in ρ. If ρ can be written in the form (42), then $\tau(\rho) = 0$, and the state is not genuinely entangled. The reverse is not true in general, i.e., even if $\tau(\rho) = 0$, the state ρ could still be genuinely entangled. The maximum value of τ can be shown to be $1/2$ [89]. An example of a state which has $\tau(\rho) = 1/2$ is the Greenberger-Horne-Zeilinger (GHZ) state $\rho_{\text{GHZ}} = |\text{GHZ}\rangle\langle\text{GHZ}|$, with $|\text{GHZ}\rangle = (|111\rangle + |222\rangle)/\sqrt{2}$ (see Ref. [37]), and the same (maximum) value of $\tau(\rho)$ is attained for so-called connected graph states [89]. The entanglement witness W_{GHZ} for the GHZ state found by the algorithm in Ref. [88] is

$$W_{\text{GHZ}} = \mathbb{1} - \frac{3}{2}\rho_{\text{GHZ}}. \tag{47}$$

In this case, we have the same $\mathcal{P}_s$ for all subsets s: $\mathcal{P}_s = (\mathbb{1} - \rho_{\text{GHZ}})/2$, with eigenvalues 0 and $\frac{1}{2}$ ($\mathbb{1} - \mathcal{P}_s$ has eigenvalues $\frac{1}{2}$ and 1). For $\mathcal{Q}_s$ we have $\mathcal{Q}_s = \frac{1}{2}\,\mathbb{1} - \rho_{\text{GHZ}}^{T_s}$ with eigenvalues 0, $\frac{1}{2}$ and 1 (same eigenvalues for $\mathbb{1} - \mathcal{Q}_s$).

We note that τ is invariant under a change of basis. In our case, this means that any basis (e.g., a helicity basis) can be used to describe the polarization vectors ϵ_j. Furthermore, due to the properties of the matrix element M_{TC}, the entanglement measure $\tau(\rho)$ is Lorentz invariant as well as gauge invariant in the sense of Eq. (22). In

principle, $\tau(\rho)$ can be measured by reconstructing the density matrix [95]. Experimentally, this can be done by conducting coincidence measurements of the emitted photons with various polarization filters, as described in Ref. [96].

Below, we calculate $\tau(\rho)$ for the same parameter values as used in Sec. III C in the calculation of the differential cross section. It is also interesting to investigate to which extent the state ρ is mixed. To this end, we have computed, in addition to $\tau(\rho)$, the von Neumann entropy $Q(\rho)$, defined as [97]

$$Q(\rho) = -\operatorname{Tr}\left(\rho \log_2(\rho)\right) = -\sum_{j=1}^{8} u_j \log_2(u_j)\,, \qquad (48)$$

where the u_j's are the eigenvalues of ρ. For any pure state $\rho = |\psi\rangle\langle\psi|$, we have $Q = 0$ because $\rho^2 = \rho$ and the eigenvalues are $u_j = 1$. A maximally mixed state ρ_{maxmix}, which has equal diagonal entries, and vanishing non-diagonal matrix elements, has $Q = (8\times\frac{1}{8})\,\log_2 8 = 3$ in the current case. $\tau(\rho_{\text{maxmix}}) = 0$, since ρ_{maxmix} can be factorized as $\rho_{\text{maxmix}} = \mathbb{1}_{2\times2}\otimes\mathbb{1}_{2\times2}\otimes\mathbb{1}_{2\times2}/8$, and is therefore not entangled.

The results of the evaluation of τ and Q are shown in Figs. 7, and 8, using the parameters of the setup described in Sec. III C (180 keV photons on a stationary target). For the calculation of the entanglement measure $\tau(\rho)$, we employ the program PPTMIXER, made available at [98] by the authors of Ref. [88]. For comparison, we also show the differential cross section summed over the final polarizations, to give an idea about whether or not the cross section and the entanglement measure τ are large at the same parameter values.

By inspecting Figs. 7 and 8, we see that, somewhat unfortunately, a large value of the entanglement measure τ is accompanied by a small value of the differential cross section. This may limit the practical usefulness of the three-photon Compton effect as a source of entangled photons. However, we note that even a small value of $\tau \neq 0$ implies that the state ρ is genuinely entangled. We also point out that it is natural for τ, as a measure of correlation, to approach zero for small $\omega_{1,2,3}$ [at the edges of the "triangle" in the $\omega_1\omega_2$ plane where the differential cross section is non-vanishing, see Figs. 7(c), 8(c) and Fig. 3]. The physical reason for the lack of entanglement is that in the limit of vanishing ω_j for one of the photons, the three-photon Compton process factorizes into a sequential process of one-photon emission followed by a two-photon event, which leads to a final state which is not entangled in all three photons. In the extreme case of two vanishing photon energies (for example, $\omega_1 \to 0$ and $\omega_2 \to 0$, but finite ω_3), the three-photon Compton process becomes a sequence of three one-photon events, again with vanishing correlation.

Finally, we note that the von Neumann entropy varies depending on the setup. In Fig. 7, we have $Q \ll 1$ in large parts of the $\omega_1\omega_2$ plane. The von Neumann entropy of the state produced in the forward cone [see Fig. 7(b)] is lower than the entropy of triplet photon states in the backward cone [Fig. 8(b)]. The entanglement measure $\tau(\rho)$ attains values close to its maximum value 1/2 in Fig. 7, indicating that close to a maximally entangled triplet photon state is produced.

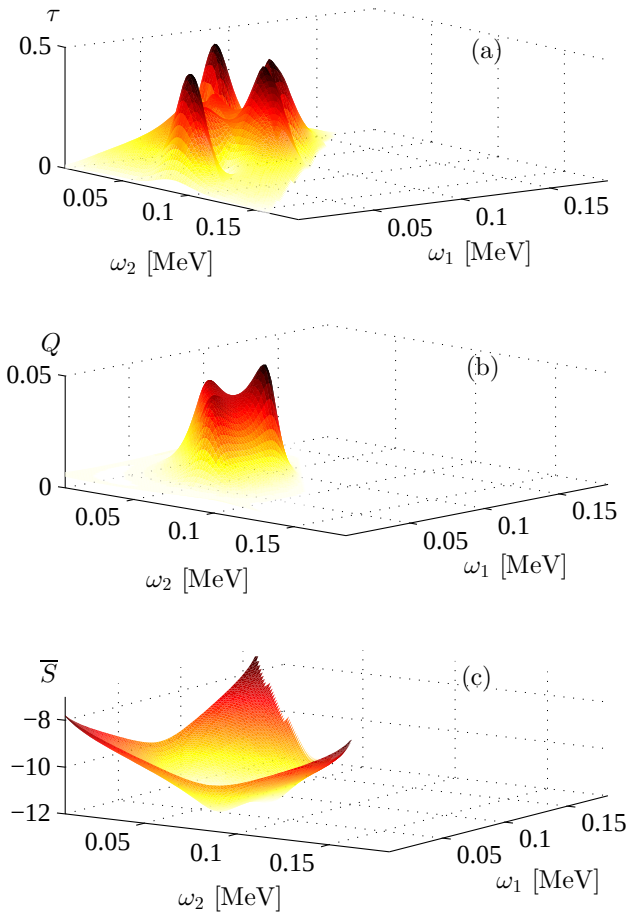

FIG. 7. (Color online) We investigate the entanglement and von Neumann entropy for the parameters given as given in Fig. 3(a). Figure (a) has the entanglement measure $\tau(\rho)$, whereas in Fig. (b) we plot the von Neumann entropy Q. For completeness, we plot in Fig. (c) the quantity $\overline{S}$ defined in Eq. (32), i.e., the decadic logarithm of the differential cross section summed over the polarizations of the emitted photons.

We have also computed entangled measures and entropies for the setup described in Sec. III D, an intense laser beam colliding with a high-energy electron beam. The results are very similar to those already presented in Figs. 7 and 8. Also in this case, a large value of τ was only found in angular regions were the cross section is small. Finally, a limited investigation for the case with $\omega_0 = 3$ MeV, $E_i = m$ was carried out. Although potentially difficult to realize experimentally, this case is interesting

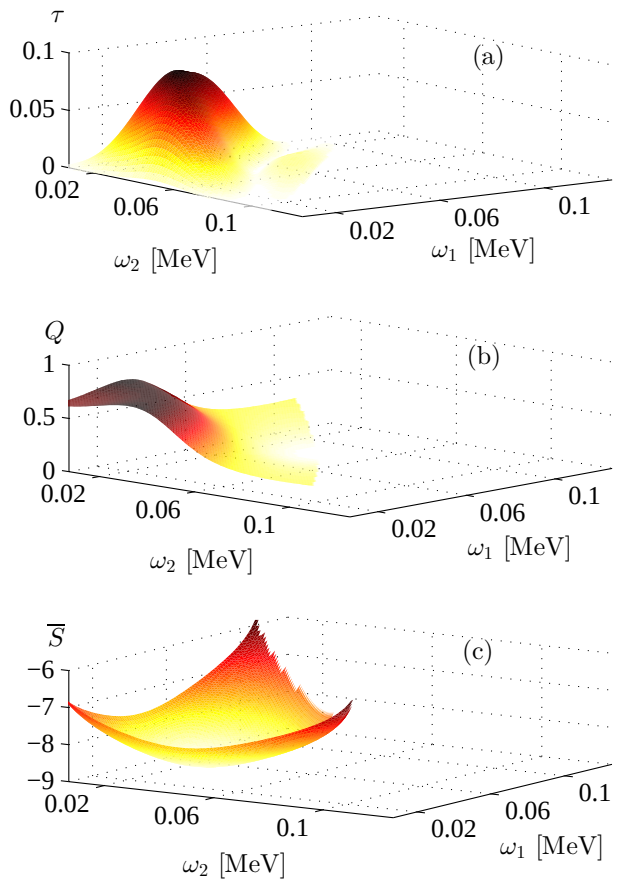

FIG. 8. (Color online) We investigate the entanglement of triple Compton photons for the parameters of Fig. 3(b), i.e., for a scattering in the backward cone as seen from the incoming photon. The entanglement measure τ and von Neumann entropy Q are plotted in Figs. (a) and (b), respectively. Finally, in Fig. (c), we plot the quantity $\overline{S}$ [see Eq. (32) for definition], i.e., the decadic logarithm of the differential cross section summed over the polarizations of the emitted photons.

since the total cross section for triple Compton scattering peaks around this value of ω_0 (see Fig. 2). However, a parameter region where both the cross section and τ are large could not be found.

V. CONCLUSIONS

We have presented a theoretical analysis of the three-photon, or triple Compton effect. Contrary to the single Compton event, the double and triple processes do not have a classical analog and therefore, a single low-energy incoming photon is not sufficient to excite a process with the emission of more than one quantum. Both the total as well as the differential cross sections for the double-Compton as well as the triple-Compton processes tend to zero for low incoming photon energy, as demonstrated in Fig. 2. The cross section vanishes also for $\omega_0/m \to \infty$, where we recall that ω_0 is the energy of the incoming photon. Because the cross sections for double and triple scattering vanish for both $\omega_0 \to 0$ and $\omega_0 \to \infty$, there has to be a certain initial photon energy for which the double and triple Compton cross sections have a maximum. With our convention for the infrared cutoff, this maximum was found to be at $\omega_0 \approx 3$ MeV for both the double and triple Compton effect.

In a previous experiment [34], the triple Compton process was studied with a symmetric detector geometry, with three detectors oriented in a "Mercedes–star" configuration with azimuth angles $\phi_j = 2j\pi/3$ for $j = 1, 2, 3$. The polar angle is assumed to be equal for all three detectors. The detectors are thus situated at the corners of an equilateral triangle. We assume this detector geometry for our cross section calculations (see Figs. 3 and 5). Supplementing a previous discussion [36], we consider two example cases for the differential cross section of the triple Compton process: 180 keV photons at stationary electrons, and laser photons of energy 2.5 eV on GeV electrons. We find that the three-photon Compton process is measurable at present synchrotron or laser facilities, and constitutes one of the most straightforward processes for the manifestation of high-energy entanglement in the quantum world. We suggest that the most favorable experimental setup for measuring the triple Compton process would be a high-flux synchrotron light source combined with stationary targets. Furthermore, as demonstrated in Fig. 7, a high degree of entanglement is reached in the final three-photon state, for an arrangement of the detectors in the forward cone, for the case of an 180 keV photon impacting on stationary electrons.

ACKNOWLEDGMENTS

This work was supported by the National Science Foundation (Grant PHY-1068547) and the National Institute of Standards and Technology (NIST precision measurement grant). E.L. acknowledges partial support from the FPR program of RIKEN.

[1] O. Klein and T. Nishina, Z. Phys. A **52**, 853 (1929).

[2] A. H. Compton, Phys. Rev. **21**, 483 (1923).

[3] J. M. Jauch and F. Rohrlich, *The Theory of Photons and Electrons*, 2 ed. (Springer, Heidelberg, 1980).
[4] C. Itzykson and J. B. Zuber, *Quantum Field Theory*, 2 ed. (Dover Publications, New York, 2006).
[5] W. E. Duncanson and C. A. Coulson, Proc. Phys. Soc. **57**, 190 (1945).
[6] A. I. Al-Sharif, Phys. Rev. A **72**, 012703 (2005).
[7] M. Hakala, K. Nygård, J. Vaara, M. Itou, Y. Sakurai, and K. Hämäläinen, J. Chem. Phys. **130**, 034506 (2009).
[8] A. Koizumi, T. Nagao, Y. Kakutani, N. Sakai, K. Hirota, and Y. Murakami, Phys. Rev. B **69**, 060401(R) (2004).
[9] C. Bellin, B. Barbiellini, S. Klotz, T. Buslaps, G. Rousse, T. Strässle, and A. Shukla, Phys. Rev. B **83**, 094117 (2011).
[10] V. Olevano, A. Titov, M. Ladisa, K. Hämäläinen, S. Huotari, and M. Holzmann, Phys. Rev. B **86**, 195123 (2012).
[11] G. R. Blumenthal and R. J. Gould, Rev. Mod. Phys. **42**, 237 (1970).
[12] M. J. Cooper, Rep. Prog. Phys. **48**, 415 (1985).
[13] S. H. Glenzer and R. Redmer, Rev. Mod. Phys. **81**, 1625 (2009).
[14] H. R. Weller, M. W. Ahmed, H. Gao, W. Tornow, Y. K. Wu, M. Gai, and R. Miskimen, Prog. Part. Nucl. Phys. **62**, 257 (2009).
[15] C. Harvey, T. Heinzl, and A. Ilderton, Phys. Rev. A **79**, 063407 (2009).
[16] F. Mackenroth, A. Di Piazza, and C. H. Keitel, Phys. Rev. Lett. **105**, 063903 (2010).
[17] D. Seipt and B. Kämpfer, Phys. Rev. A **83**, 022101 (2011).
[18] C. Bula, K. T. McDonald, E. J. Prebys, C. Bamber, S. Boege, T. Kotseroglou, A. C. Melissinos, D. D. Meyerhofer, W. Ragg, D. L. Burke, R. C. Field, G. Horton-Smith, A. C. Odian, J. E. Spencer, D. Walz, S. C. Berridge, W. M. Bugg, K. Shmakov, and A. W. Weidemann, Phys. Rev. Lett. **76**, 3116 (1996).
[19] M. Babzien, I. Ben-Zvi, K. Kusche, I. V. Pavlishin, I. V. Pogorelsky, D. P. Siddons, V. Yakimenko, D. Cline, F. Zhou, T. Hirose, Y. Kamiya, T. Kumita, T. Omori, J. Urakawa, and K. Yokoya, Phys. Rev. Lett. **96**, 054802 (2006).
[20] J. Felsteiner and P. Pattison, Nucl. Instrum. Methods **173**, 323 (1980).
[21] F. Mandl and T. H. R. Skyrme, Proc. Roy. Soc. London, Ser. A **215**, 497 (1952).
[22] P. E. Cavanagh, Phys. Rev. **87**, 1131 (1952).
[23] M. R. McGie, F. P. Brady, and W. J. Knox, Phys. Rev. **152**, 1190 (1966).
[24] B. S. Sandhu, R. Dewan, B. Singh, and B. S. Ghumman, Phys. Rev. A **60**, 4600 (1999).
[25] B. S. Sandhu, R. Dewan, M. B. Saddi, B. Singh, and B. S. Ghumman, Nucl. Instrum. Methods Phys. Res. B **168**, 329 (2000).
[26] M. B. Saddi, B. S. Sandhu, and B. Singh, Ann. Nucl. Ener. **33**, 271 (2006).
[27] M. B. Saddi, B. Singh, and B. S. Sandhu, Nucl. Instrum. Methods Phys. Res. B **266**, 3309 (2008).
[28] M. B. Saddi, B. Singh, and B. S. Sandhu, Nucl. Tech. **175**, 168 (2011).
[29] M. Ram and P. Y. Wang, Phys. Rev. Lett. **26**, 476 (1971), [Erratum Phys. Rev. Lett. **26**, 1210 (1971)].
[30] E. Lötstedt and U. D. Jentschura, Phys. Rev. Lett. **103**, 110404 (2009).
[31] E. Lötstedt and U. D. Jentschura, Phys. Rev. A **80**, 053419 (2009).
[32] D. Seipt and B. Kämpfer, Phys. Rev. D **85**, 101701 (2012).
[33] F. Mackenroth and A. Di Piazza, e-print arXiv:1208.3424v1 [hep-ph], 2012.
[34] M. R. McGie and F. P. Brady, Phys. Rev. **167**, 1186 (1968).
[35] R. C. Majumdar, V. S. Mathur, and J. Dhar, Nuovo Cimento **12**, 97 (1959).
[36] E. Lötstedt and U. D. Jentschura, Phys. Rev. Lett. **108**, 233201 (2012).
[37] D. M. Greenberger, M. A. Horne, A. Shimony, and A. Zeilinger, Am. J. Phys. **58**, 1131 (1990).
[38] T. E. Keller, M. H. Rubin, Y. Shih, and L.-A. Wu, Phys. Rev. A **57**, 2076 (1998).
[39] J.-W. Pan, D. Bouwmeester, M. Daniell, H. Weinfurter, and A. Zeilinger, Nature (London) **403**, 515 (2000).
[40] M. Eibl, S. Gaertner, M. Bourennane, C. Kurtsiefer, M. Żukowski, and H. Weinfurter, Phys. Rev. Lett. **90**, 200403 (2003).
[41] F. Gravier and B. Boulanger, J. Opt. Soc. Am. B **25**, 98 (2008).
[42] J. Wen, E. Oh, and S. Du, J. Opt. Soc. Am. B **27**, A11 (2010).
[43] H. Hübel, D. R. Hamel, A. Fedrizzi, S. Ramelow, K. J. Resch, and T. Jennewein, Nature (London) **466**, 601 (2010).
[44] D. A. Antonosyan, T. V. Gevorgyan, and G. Yu. Kryuchkyan, Phys. Rev. A **83**, 043807 (2011).
[45] M. Corona, K. Garay-Palmett, and A. B. U'Ren, Opt. Lett. **36**, 190 (2011).
[46] A. Dot, A. Borne, B. Boulanger, K. Bencheikh, and J. A. Levenson, Phys. Rev. A **85**, 023809 (2012).
[47] S. N. Gupta, Phys. Rev. **96**, 1453 (1954).
[48] S. N. Gupta, Phys. Rev. **98**, 1502 (1955).
[49] F. A. Berends and R. Gastmans, Nucl. Phys. B **61**, 414 (1973).
[50] F. A. Berends and R. Kleiss, Nucl. Phys. B **186**, 22 (1981).
[51] O. Adriani *et al.* [L3 Collaboration], Phys. Lett. B **288**, 404 (1992).
[52] A. Zerwekh, C. Dib, and R. Rosenfeld, Phys. Lett. B **549**, 154 (2002).
[53] W. Bernreuther, U. Löw, J. P. Ma, and O. Nachtmann, Z. Phys. C **41**, 143 (1988).
[54] B. K. Arbic, S. Hatamian, M. Skalsey, J. Van House, and W. Zheng, Phys. Rev. A **37**, 3189 (1988).
[55] M. Skalsey and J. Van House, Phys. Rev. Lett. **67**, 1993 (1991).
[56] P. A. Vetter and S. J. Freedman, Phys. Rev. Lett. **91**, 263401 (2003).
[57] T. Yamazaki, T. Namba, S. Asai, and T. Kobayashi, Phys. Rev. Lett. **104**, 083401 (2010).
[58] F. M. Abel, G. S. Adkins, and T. J. Yoder, Phys. Rev. A **83**, 062502 (2011).
[59] A. Ore and J. Powell, Phys. Rev. **75**, 1696 (1949).
[60] W. E. Caswell, G. P. Lepage, and J. Sapirstein, Phys. Rev. Lett. **38**, 488 (1977).
[61] G. S. Adkins, R. N. Fell, and J. Sapirstein, Ann. Phys. (N.Y.) **295**, 136 (2002).
[62] B. A. Kniehl, A. V. Kotikov, and O. L. Veretin, Phys. Rev. Lett. **101**, 193401 (2008).
[63] G. S. Adkins, D. R. Droz, D. Rastawicki, and R. N. Fell,

Phys. Rev. A **81**, 042507 (2010).
[64] S. Asai, S. Orito, and N. Shinohara, Phys. Lett. B **357**, 475 (1995).
[65] O. Jinnouchi, S. Asai, and T. Kobayashi, Phys. Lett. B **572**, 117 (2003).
[66] C. I. Westbrook, D. W. Gidley, R. S. Conti, and A. Rich, Phys. Rev. Lett. **58**, 1328 (1987).
[67] C. I. Westbrook, D. W. Gidley, R. S. Conti, and A. Rich, Phys. Rev. A **40**, 5489 (1989).
[68] J. S. Nico, D. W. Gidley, A. Rich, and P. W. Zitzewitz, Phys. Rev. Lett. **65**, 1344 (1990).
[69] R. S. Vallery, P. W. Zitzewitz, and D. W. Gidley, Phys. Rev. Lett. **90**, 203402 (2003).
[70] L. M. Brown and R. P. Feynman, Phys. Rev. **85**, 231 (1952).
[71] V. V. Sudakov, Zh. Éksp. Teor. Fiz. **30**, 87 (1956), [Sov. Phys. JETP **3**, 65 (1956)].
[72] D. R. Yennie, S. C. Frautschi, and H. Suura, Ann. Phys. (N.Y.) **13**, 379 (1961).
[73] K. J. Mork, Phys. Rev. A **4**, 917 (1971).
[74] S. Schnez, E. Lötstedt, U. D. Jentschura, and C. H. Keitel, Phys. Rev. A **75**, 053412 (2007).
[75] W. H. Press, B. P. Flannery, S. A. Teukolsky, and W. T. Vetterling, *Numerical Recipes in C: The Art of Scientific Computing*, 2 ed. (Cambridge University Press, Cambridge, UK, 1993).
[76] H. Hu, C. Müller, and C. H. Keitel, Phys. Rev. Lett. **105**, 080401 (2010).
[77] A. Di Piazza and K. Z. C. H. K. Hatsagortsyan, Phys. Rev. Lett. **105**, 220403 (2010).
[78] K. J. Mork, Phys. Rev. **160**, 1065 (1967).
[79] S. Jarp and K. J. Mork, Phys. Rev. D **8**, 159 (1973).
[80] R. J. Gould, Astrophys. J. **285**, 275 (1984).
[81] T. Sattler, T. Tschentscher, J. R. Schneider, M. Vos, A. S. Kheifets, D. R. Lun, E. Weigold, G. Dollinger, H. Bross, and F. Bell, Phys. Rev. B **63**, 155204 (2001).
[82] D. L. Burke, R. C. Field, G. Horton-Smith, J. E. Spencer, D. Walz, S. C. Berridge, W. M. Bugg, K. Shmakov, A. W. Weidemann, C. Bula, K. T. McDonald, E. J. Prebys, C. Bamber, S. J. Boege, T. Koffas, T. Kotseroglou, A. C. Melissinos, D. D. Meyerhofer, D. A. Reis, and W. Ragg, Phys. Rev. Lett. **79**, 1626 (1997).
[83] A. Di Piazza, C. Müller, K. Z. Hatsagortsyan, and C. H. Keitel, Rev. Mod. Phys. **84**, 1177 (2012).
[84] A. Ilderton, Phys. Rev. Lett. **106**, 020404 (2011).
[85] M. Seevinck and J. Uffink, Phys. Rev. A **65**, 012107 (2001).
[86] G. Tóth, O. Gühne, M. Seevinck, and J. Uffink, Phys. Rev. A **72**, 014101 (2005).
[87] J.-D. Bancal, N. Gisin, Y.-C. Liang, and S. Pironio, Phys. Rev. Lett. **106**, 250404 (2011).
[88] B. Jungnitsch, T. Moroder, and O. Gühne, Phys. Rev. Lett. **106**, 190502 (2011).
[89] B. Jungnitsch, T. Moroder, and O. Gühne, Phys. Rev. A **84**, 032310 (2011).
[90] N. Brunner, J. Sharam, and T. Vértesi, Phys. Rev. Lett. **108**, 110501 (2012).
[91] G. Tóth, Phys. Rev. A **85**, 022322 (2012).
[92] J.-Y. Wu, H. Kampermann, D. Bruß, C. Klöckl, and M. Huber, Phys. Rev. A **86**, 022319 (2012).
[93] M. Lewenstein, B. Kraus, J. I. Cirac, and P. Horodecki, Phys. Rev. A **62**, 052310 (2000).
[94] J. F. Sturm, Opt. Meth. Softw. **11**, 625 (1999).
[95] J. Fan, M. D. Eisaman, and A. Migdall, Opt. Express **15**, 18339 (2007).
[96] D. F. V. James, P. G. Kwiat, W. J. Munro, and A. G. White, Phys. Rev. A **64**, 052312 (2001).
[97] A. Wehrl, Rev. Mod. Phys. **50**, 221 (1978).
[98] See the URL `http://www.mathworks.com/matlabcentral/fileexchange/30968`.